An investigation into reinforced and functionally graded lattice structures

Journal Title
XX(X):1–9

DOI: 10.1177/ToBeAssigned
www.sagepub.com/
SAGE

Ian Maskery[1], Alexandra Hussey[1], Ajit Panesar[1], Adedeji Aremu[1], Christopher Tuck[1], Ian Ashcroft[1] and Richard Hague[1]

Abstract

Lattice structures are regarded as excellent candidates for use in lightweight energy absorbing applications, such as crash protection. In this paper we investigate the crushing behaviour, mechanical properties and energy absorption of lattices made by an additive manufacturing (AM) process. Two types of lattice were examined; body-centred-cubic (BCC) and a reinforced variant called BCC_z. The lattices were subject to compressive loads in two orthogonal directions, allowing an assessment of their mechanical anisotropy to be made. We also examined functionally graded versions of these lattices, which featured a density gradient along one direction. The graded structures exhibited distinct crushing behaviour, with a sequential collapse of cellular layers preceding full densification. For the BCC_z lattice, the graded structures were able to absorb around 114% more energy per unit volume than their non-graded counterparts before full densification, 1371 ± 9 kJ/m^3 vs. 640 ± 10 kJ/m^3. This highlights the strong potential for functionally graded lattices to be used in energy absorbing applications. Finally, we determined several of the Gibson-Ashby coefficients relating the mechanical properties of lattice structures to their density; these are crucial in establishing the constitutive models required for effective lattice design. These results improve the current understanding of AM lattices, and will enable the design of sophisticated, functional, lightweight components in the future.

Keywords

selective laser sintering, additive manufacture, lattice, functional grading, energy absorption, mechanical testing

Introduction

Porous metal foams and, more recently, regularly repeating lattices, have been investigated for use in applications including structural lightweighting, thermal transfer, and impact and blast protection.[1–7] Additive manufacturing (AM) now provides a means to produce lattices with almost complete geometric freedom, and with a level of control over the volume fraction and repeating cell size which is unachievable for foams. Also, through the range of AM processes available, these structures can be made in a wide range of materials, including polymers and metal alloys, and at a range of length scales from sub-millimeter to several meters.

This makes AM an attractive route to a new generation of lightweight functional components that incorporate lattices based on multi-objective topology optimisation (MTO).[8–11] Latticed AM components designed in this way will be material-efficient and will offer superior functionality over those they replace; an optimised component can benefit from enhanced convective cooling thanks to the large surface area of an embedded lattice,[12,13] and the same lattice can absorb the impact energy of a projectile, for example in protection equipment such as armour.[14,15]

For a combined lattice and MTO design approach to be used effectively, it must incorporate constitutive models relating the distribution of the lattice material and the resulting physical performance. These models must be informed, and validated, by experiment. The purpose of the research laid out here is to gain insight into the performance of two variants of AM lattice, body-centred-cubic (BCC)

[1]Additive Manufacturing & 3D Printing Research Group, Faculty of Engineering, University of Nottingham, Nottingham NG7 2RD, UK

Corresponding author:
Ian Maskery, Additive Manufacturing & 3D Printing Research Group, Faculty of Engineering, University of Nottingham, Nottingham NG7 2RD, UK

Email: ian.maskery@nottingham.ac.uk

and z-reinforced body-centred-cubic (BCC$_z$), and assess this with the pre-existing models of Gibson and Ashby.[1]

Our investigation also includes lattice structures featuring a density gradient. These graded structures are representative of those we can expect from a combined lattice and MTO design approach, where spatially varying material properties are required. Understanding the deformation and energy absorption processes of these graded structures, and how they compare to those of non-graded lattices, provides the main motivation for this work and will inform the future design process for lightweight functionally graded parts.

Previous investigations of graded density cellular structures have focussed mainly on graded foams[16–20] and honeycombs.[21,22] Brothers and Dunand[17] compared the mechanical properties of graded density aluminium foam with those of a foam of uniform density. They showed that the graded foam exhibited a plateau stress which rose smoothly with increasing strain, which they took to be consistent with the progressive deformation of low- to high-density regions. This was in comparison to the near constant plateau stress of the non-graded foam. In a novel investigation of functionally graded Polylactide (PLA) foams, Mosanenzadeh et al[23] examined the acoustic absorption capability of foams with various cell sizes and distributions, showing that graded foams can significantly outperform uniform foams in terms of their average and maximum absorption coefficients. In another relevant study, van Grunsven et al[24] examined a graded density Ti6Al-4V lattice structure made by electron beam melting (EBM). Van Grunsven et al[24] suggested that the progressive deformation and collapse of increasingly dense layers could be useful in applications such as surgical implants and could offer protection from dynamic loads.

In this paper, we build on previous investigations into graded structures by examining video recordings of their deformation, and correlating the collapse processes with features in the stress-strain curves. We compare the energy absorption of graded and non-graded lattices, and provide the energy absorption per unit volume up to densification, W_{V_D}, which can be a key criterion in the selection of a lattice for a given impact protection application. Lastly, through the use of the Gibson-Ashby relationships, we empirically determine several parameters for BCC and BCC$_z$ lattices that enable informed decisions about their density to be made in future designs.

The Gibson-Ashby model of lattice deformation

Gibson and Ashby et al[1,2] examined the properties of cellular solids extensively, and provided a series of equations relating their design (principally their relative density, ρ^*) to their physical properties. Those relationships relevant to this work are reproduced in equations 1a-1c, while the associated nomenclature, used throughout this paper, is provided in table 1.

Conventional uniformly dense open-cell foams and lattices are known to undergo compressive deformation in three successive stages. The first is a linear elastic region, where the modulus, $E_{latt.}$, is roughly proportional to the square of the relative density, as given in equation 1a. If the cell walls are composed of an elastic-plastic material, the structure will develop plastic hinges, and the next regime will be a long plateau at constant stress, $\sigma_{pl.\ latt.}$. $\sigma_{pl.\ latt.}$ is known as the plastic collapse strength or plateau stress, and is related to the relative density by equation 1b. It is this long plastic plateau that makes lattices particularly attractive for the purpose of impact protection, as it contributes the majority of the energy absorption under compressive loading. Also, as $\sigma_{pl.\ latt.}$ is directly controllable through equation 1b, the plateau stress can be chosen to be just below that which would cause damage to the protected object, thus providing maximal energy absorption whilst protection is maintained. Finally, the structure will enter the densification regime, where the individual cell walls or struts come into contact with one another and provide a drastically increased stiffness. This occurs at the densification strain, ε_D, which is given in equation 1c. For the prefactors C_1 and C_5 in equations 1a and 1b, the range of values given by Gibson and Ashby et al[1,2] are 0.1 - 4.0 and 0.25 - 0.35, respectively, while the exponents n and m are ~ 2 and $\sim 3/2$, respectively. Regarding equation 1c, the value of α varies between 1.4 and 2.0.[1,2]

$$\frac{E_{latt.}}{E_{\text{sol.}}} = C_1 \left(\frac{\rho_{latt.}}{\rho_{sol.}} \right)^n, \tag{1a}$$

$$\frac{\sigma_{pl.\ latt.}}{\sigma_{ys\ sol.}} = C_5 \left(\frac{\rho_{latt.}}{\rho_{sol.}} \right)^m, \tag{1b}$$

$$\varepsilon_D = 1 - \alpha \left(\frac{\rho_{latt.}}{\rho_{sol.}} \right). \tag{1c}$$

It is clear from equations 1a, 1b and 1c that the prefactors C_1, C_5 and α play a significant role in determining the mechanical properties and deformation behaviour of lattice structures. For applications demanding high modulus, high strength and a long plastic plateau for the purpose of energy absorption, it is preferable for C_1 and C_5 to take larger values and for α to take a low value. In practice, these values, and the exponents n and m, will be determined by the physical properties of the structure; it will therefore be the task of the

Table 1. Physical and mechanical properties used in the description of lattices under compression.

Notation	Physical or mechanical property
$\rho_{latt.}$	Density of the lattice
$\rho_{sol.}$	Density of the material constituting the lattice struts or walls
ρ^*	Relative density of the lattice, equal to $\rho_{latt.}/\rho_{sol.}$
$E_{latt.}$	Elastic modulus of the lattice
$E_{sol.}$	Elastic modulus of the lattice material
E^*	Relative elastic modulus of the lattice, equal to $E_{latt.}/E_{sol.}$
$\sigma_{latt.}$	Effective stress of the lattice structure
$\sigma_{pl.\ latt.}$	Plastic collapse strength, or plateau stress, of the lattice
$\sigma_{y\ sol.}$	Yield strength of the lattice material
σ^*	Relative collapse strength of the lattice, equal to $\sigma_{pl.\ latt.}/\sigma_{y\ sol.}$
$\varepsilon_{latt.}$	Effective strain of the lattice structure
$\varepsilon_{pl.\ latt.}$	Lattice strain at plastic collapse
ε_D	Densification strain of the lattice
W_V	Energy absorbed per unit volume by the lattice under deformation
W_{V_D}	Total energy absorbed per unit volume by the lattice up to densification

designer of the latticed component, using information such as will be provided in this paper, to select the appropriate lattice type and material to meet the requirements of the target application.

Experimental details

Specimen fabrication

A series of BCC and BCC$_z$ lattice test specimens were designed with dimensions $30 \times 30 \times 30$ mm. The lattice cells were $5 \times 5 \times 5$ mm, meaning the structures each contained a $6 \times 6 \times 6$ arrangement of cells. This can be seen in the CAD representations of the structures shown in figure 1(b). The cylindrical cellular struts comprising the lattices were assigned thicknesses corresponding to relative densities, or volume fractions, of 0.19. The strut thicknesses for the BCC and BCC$_z$ cells were approximately 1.2 mm and 1.1 mm, respectively, with the latter being thinner because more of them, the additional vertical reinforcing struts, contribute to the mass of the cell. For the graded density lattices, the six layers in the xy plane were each assigned a different relative density, corresponding to a linear decrease from 0.263 at the base to 0.117 at the top. The average of these densities was 0.19, thereby allowing the graded and non-graded structures to be compared on an equal mass basis. Note that throughout this paper the z direction will refer to the direction in which the specimens were manufactured, with 'bases' and 'tops' indicating the layers at the beginning and end of the selective laser sintering (SLS) process, respectively.

The specimens were manufactured by SLS on an EOS P100 machine from polyamide PA 2200 (nylon 12). The relevant SLS processing parameters are provided in table 2. Photographs of the graded density structures are shown in figure 2, where the relative densities, ρ^*, of each layer are also provided.

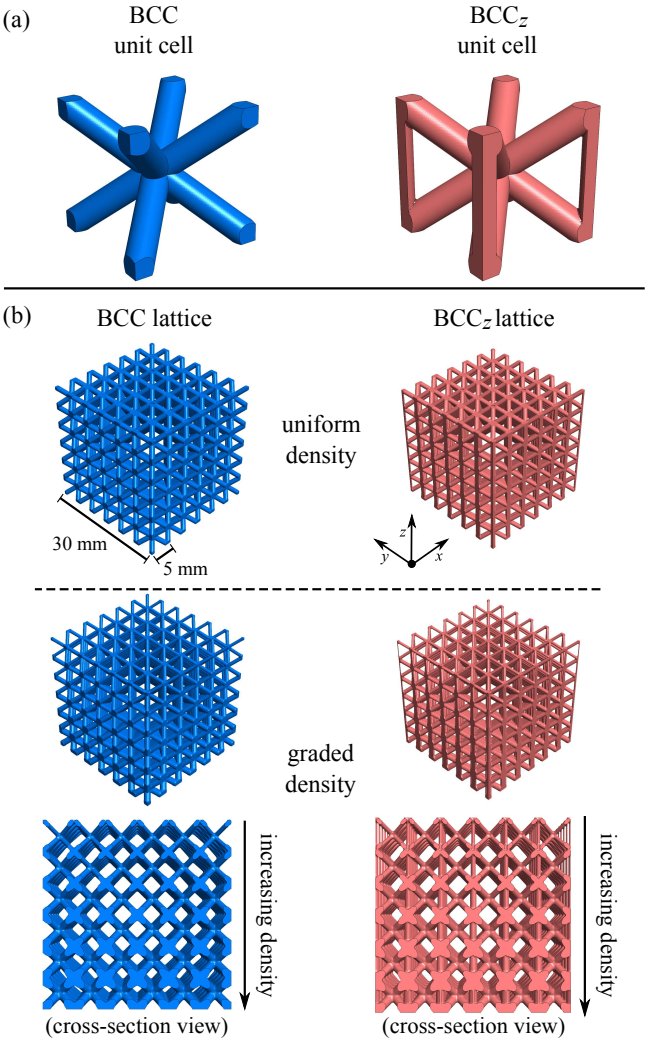

Figure 1. CAD models of the BCC and BCC$_z$ unit cells (a) and lattice structures (b). For the lattices in (b), both the uniform density (top) and graded density (bottom) instances are shown.

Table 2. SLS parameters used in the production of the BCC and BCC$_z$ lattice structures.

SLS parameter	
Laser power	21 W
Laser scan speed	2500 mm s^{-1}
Laser hatch spacing	250 μm
Powder bed temperature	173 °C
Powder deposition thickness	100 μm

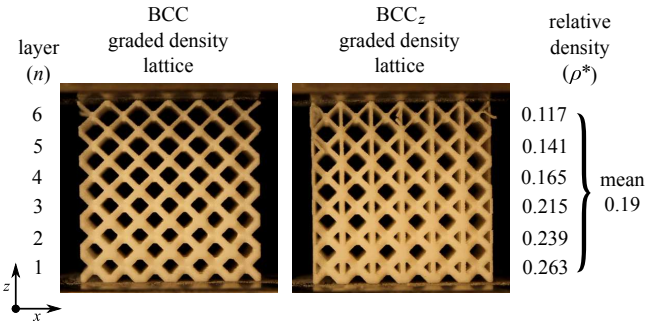

Figure 2. BCC (left) and BCC$_z$ (right) graded lattice structures. The layer numbers and associated relative densities of each layer are provided.

Mechanical testing

Mechanical testing of the lattice specimens was carried out using an Instron 5966 universal testing machine equipped with a 10 kN load cell. The compressive loads were applied at a rate of 0.25 mm s^{-1}, and a video camera was used to monitor the deformation of the lattice structures during the tests. The relatively slow compression rate was selected to ensure that structural and cellular deformation was recorded in adequate detail by the video camera. Individual frames were extracted from the deformation videos and are presented in the next section to illustrate the mechanisms of progressive collapse in the structures.

The uniform density lattice specimens were subject to compression in the z and x directions (see figure 1) to examine the mechanical anisotropy of BCC and BCC$_z$ lattice types. The graded density lattices were tested in the direction of their grading only, i.e. the z direction, in order to provide a comparison between the performance of graded and non-graded structures.

Results and discussion

Before the lattice deformation and stress-strain data are presented, some additional nomenclature must be established. Figures 3, 4, and 6 refer to 'lattice strain' or include $\varepsilon_{latt.}$ as an axis label. These are the same property and are simply the effective total strain experienced by the lattice structure, i.e. as if it were a uniform 30 × 30 × 30 mm specimen of arbitrary material. It is important to clarify this point so as to avoid confusion with the strains in individual cellular struts. Likewise, $\sigma_{latt.}$ is the effective stress of the whole structure, and does not refer to actual stress in the struts. This is the conventional way that lattice and foam structures have been analysed since the early work of Gibson and Ashby,[1] and allows straightforward identification of the key features of foam and lattice compression; initial elasticity, plastic plateau and densification.

Uniform density lattice structures

Figure 3 provides video frames from the compression of BCC and BCC$_z$ lattices at several levels of lattice strain: $\varepsilon_{latt.}$ = 0%, 15%, 30%, 45% and 60%. The deformation processes of both structure types were quite similar. From the lateral view afforded to the video camera they showed fairly uniform compression across the zx plane.

The stress-strain curves in figure 4 elucidate the BCC and BCC$_z$ lattice deformation processes. The structures exhibit linear elastic behaviour at low strain, with the gradients of the stress-strain curves in these regions providing the lattice moduli, $E_{latt.}$. The linearity terminates at the plastic collapse, which has an associated strain, $\varepsilon_{pl.\,latt.}$, and strength, $\sigma_{pl.\,latt.}$. Following plastic collapse are long plastic plateaux, which extend up to the densification strain, ε_D. The determined values of the parameters discussed above are provided in tables 3 and 5. ε_D were determined using the energy efficiency method outlined by Miltz and Ramon[25] and Li et al.[26]

The BCC$_z$ lattices, with their additional cellular reinforcing struts in the z direction, provided higher modulus and plastic collapse strength than the BCC lattices. Their modulus and plastic collapse strength were around 220% and 41% larger, respectively, than those of the BCC lattice when the compressive load was applied in the z direction. Conversely, when the load was applied perpendicularly to the reinforcing struts, in the x direction, the modulus of the BCC$_z$ structures was reduced to slightly below that of the BCC, and the plastic collapse strength was significantly diminished. The direction of the applied compressive load was seen to have little effect on the mechanical properties of the BCC lattice; this is evident in figure 4(a) where the stress-strain curves corresponding to z and x loading are almost indistinguishable. This mechanical isotropy in the z and x loading directions was to be expected because of the planar symmetry of the BCC cells in the xy, yz and zx planes. This symmetry is absent for the BCC$_z$ cells.

The compressive modulus and yield strength of the lattice strut material (PA 2200) were found by Ngim et al[27] to be 741 MPa and 55 MPa, respectively; these constitute $E_{sol.}$ and $\sigma_{ys\ sol.}$ of the Gibson-Ashby scaling relations given in

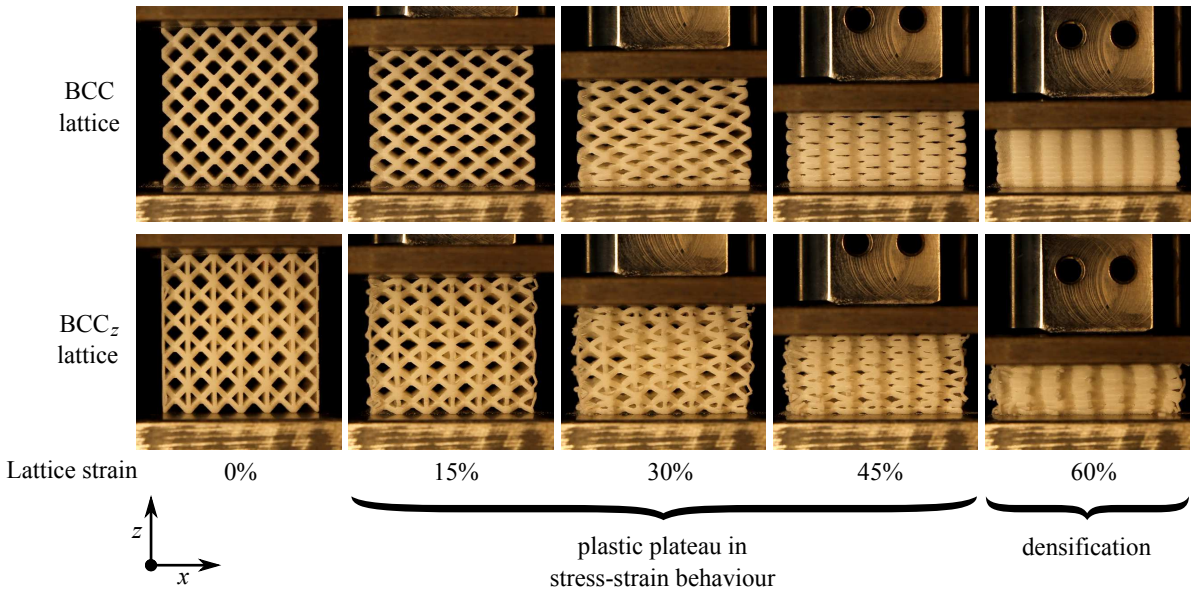

Figure 3. Frames from the video capture of BCC and BCC$_z$ lattices under compression. 'Plastic plateau' and 'densification' refer to characteristic features observed in the stress-strain behaviour of the structures - see figure 4.

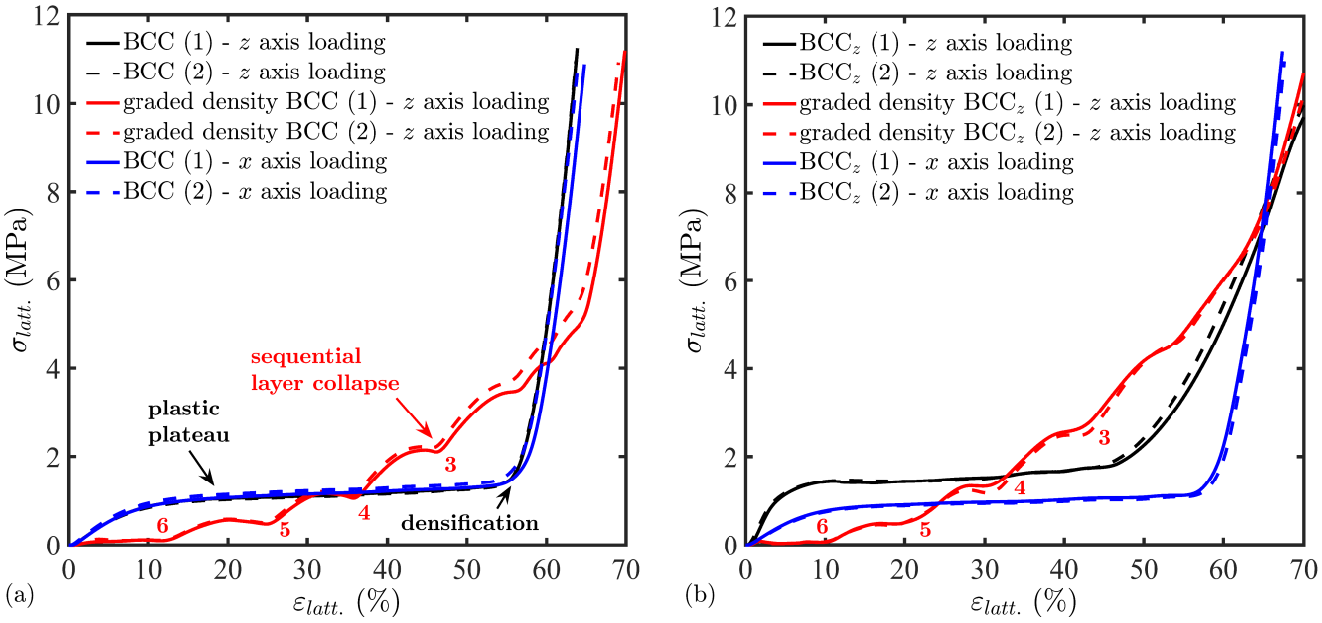

Figure 4. Compressive stress-strain curves of the BCC (a) and BCC$_z$ (b) lattice structures. The numbers 6, 5, 4, 3 indicate the collapse of lattice layers of the graded structures (see figure 2). The notation (1) and (2) in the legend refers to two samples of the same type, i.e. repeat tests.

Table 3. Mechanical properties (elastic modulus, plastic collapse strength and strain at plastic collapse) for BCC and BCC$_z$ lattice structures loaded in their z and x directions.

	BCC		BCC$_z$	
	z axis loading	x axis loading	z axis loading	x axis loading
$E_{latt.}$ (MPa)	11.8 ± 0.3	12.6 ± 0.4	37.54 ± 0.08	11.1 ± 0.2
$E^* \times 10^{-3}$	15.9 ± 0.4	17.0 ± 0.5	50.7 ± 0.1	15.0 ± 0.3
$\sigma_{pl.\ latt.}$ (MPa)	0.92 ± 0.01	0.97 ± 0.04	1.30 ± 0.01	0.806 ± 0.007
$\sigma^* \times 10^{-3}$	16.7 ± 0.2	17.6 ± 0.7	23.6 ± 0.2	14.7 ± 0.1
$\varepsilon_{pl.\ latt.}$ (%)	8.25 ± 0.01	8.19 ± 0.07	4.15 ± 0.09	7.82 ± 0.08

equations 1a and 1b. Using these to normalise the values of $E_{latt.}$ and $\sigma_{pl.\ latt.}$ determined in this work yields the relative lattice properties E^* and σ^*, which are provided in table 3. From these, and the relative density of the lattices, which is 0.19, we can estimate the Gibson-Ashby coefficients C_1,

Table 4. Gibson-Ashby coefficients for BCC and BCC$_z$ lattice structures loaded in their build direction (along the z axis).

	BCC	BCC$_z$
C_1	0.44 ± 0.01	1.404 ± 0.003
C_5	0.202 ± 0.002	0.285 ± 0.002
α	2.449 ± 0.002	2.87 ± 0.04

C_5 and α of equations 1a, 1b and 1c, assuming $n = 2$ and $m = 3/2$. These are provided in table 4.

For both BCC and BCC$_z$ lattice types, the determined values of C_1 lie in the range of 0.1 - 4.0 previously given by Gibson and Ashby.[2] For the prefactor C_5, only the value determined for the BCC$_z$ lattice conforms to Gibson and Ashby's[2] range of 0.25 - 0.35. The value of C_5 for the BCC lattice was lower, at 0.202 ± 0.002, meaning that the plateaux strengths were slightly lower than might be predicted by Gibson and Ashby's $\sigma^* = C_5\ \rho^{*3/2}$ relationship.[1] However, it must be acknowledged that while the exponent $m = 3/2$ was used here, it too is known to vary from one lattice or foam type to another, perhaps taking values up to 2. Similarly, the determined values of α for both lattice types lie above the range of 1.4 - 2.0 given by Gibson and Ashby,[2] meaning that the densification strains observed here are lower than might be predicted. An investigation including a range of lattice structures of varying density could explicitly determine C_1, C_5, n, m and α for a given lattice type and material, but this is beyond the remit of this paper.

Graded density lattice structures

The deformation processes of the graded density BCC and BCC$_z$ lattice structures are illustrated in figure 5, which shows a series of video frames from the compressive tests. For both lattice cell types the deformation processes are similar. Beginning with the lowest density layers at the tops of the structures, the lattices deform in a sequence of layer collapses, each with its own linear elastic region, plastic collapse and short plastic plateau. These are evident in the stress-strain curves of figure 4.

For the graded BCC and BCC$_z$ lattices, the collapse of the first four layers (those denoted $n = 6, 5, 4$ and 3 in figure 2) are easily identified in the compression video frames and are distinct in the stress-strain curves. However, the collapse of the final two layers ($n = 2$ and 1 in figure 2) are more difficult to resolve. The corresponding stress-strain curves for the graded lattices suggest this is because the collapse of the final layers occurs just shortly before, or concurrently with, the onset of global densification; therefore, many of the neighbouring cellular struts in the lattice are in direct contact, leading to significantly increased stiffness which obscures the collapse of layers 2 and 1.

Energy absorption

The cumulative energy absorption per unit volume, W_V, of the lattice structures under compressive deformation were calculated by numerically integrating the stress-strain curves. These are provided in figure 6 for both the BCC and BCC$_z$ lattices. The total energies per unit volume absorbed by the lattices up to densification were calculated and are presented, along with the densification strains for each structure, in table 5.

The W_V behaviour of the non-graded BCC lattices in figure 6(a) show long linear regions that are directly proportional to the lattice strain. These correspond to the plastic plateaux seen in the stress-strain behaviour and so extend from the plastic collapse point, at around 8% strain, up to densification, at around 53% strain. After densification, W_V exhibit turning points to steeper gradients; this can be attributed to the much increased structural stiffness after this point. As observed previously in the stress-strain curves, there was very little difference in the W_V curves of the BCC structures loaded parallel and perpendicular to their build direction (the z direction). The total energies absorbed up to densification for these conditions were 529 ± 6 kJ/m^3 and 570 ± 10 kJ/m^3, respectively.

In contrast to the non-graded BCC lattices, the graded structures exhibited non-linear W_V behaviour, in which W_V were roughly proportional to $\varepsilon_{latt.}{}^3$. They absorbed much less energy per unit volume than the non-graded structures at low strain, during the successive collapse of the weaker, low density, cells, but this increased rapidly so that at around 52% strain the energy absorbed by graded and non-graded structures was equal. This difference in W_V behaviour, and the higher densification strain for graded structures, led to the graded lattice structures absorbing more energy before full densification. They absorbed 940 ± 50 kJ/m^3, which is (80 ± 10)% more than the non-graded structures.

Very similar behaviour was observed for the energy absorption of the BCC$_z$ lattices, as shown in figure 6(b). The non-graded structures showed linear dependence of W_V on the strain and, as in the stress-strain curves, there was reduced performance, i.e. lower energy absorption, when the BCC$_z$ lattices were loaded perpendicularly to their reinforced direction. Even though the densification strain of the perpendicularly loaded structures was higher than those loaded in the reinforced direction, their energy absorption at densification was around 24% lower. The graded BCC$_z$ structures also absorbed more energy up to densification

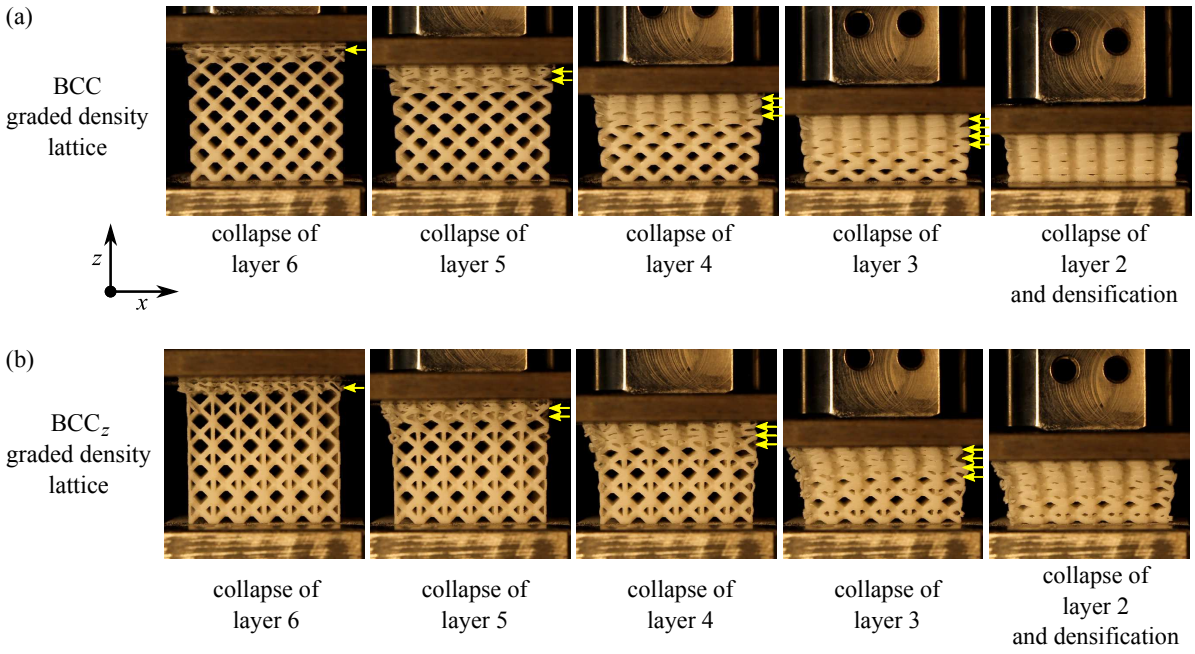

Figure 5. Frames from the videos of a graded density BCC lattice (a) and BCC$_z$ lattice (b) under compression. Arrows indicate the collapse of successive layers.

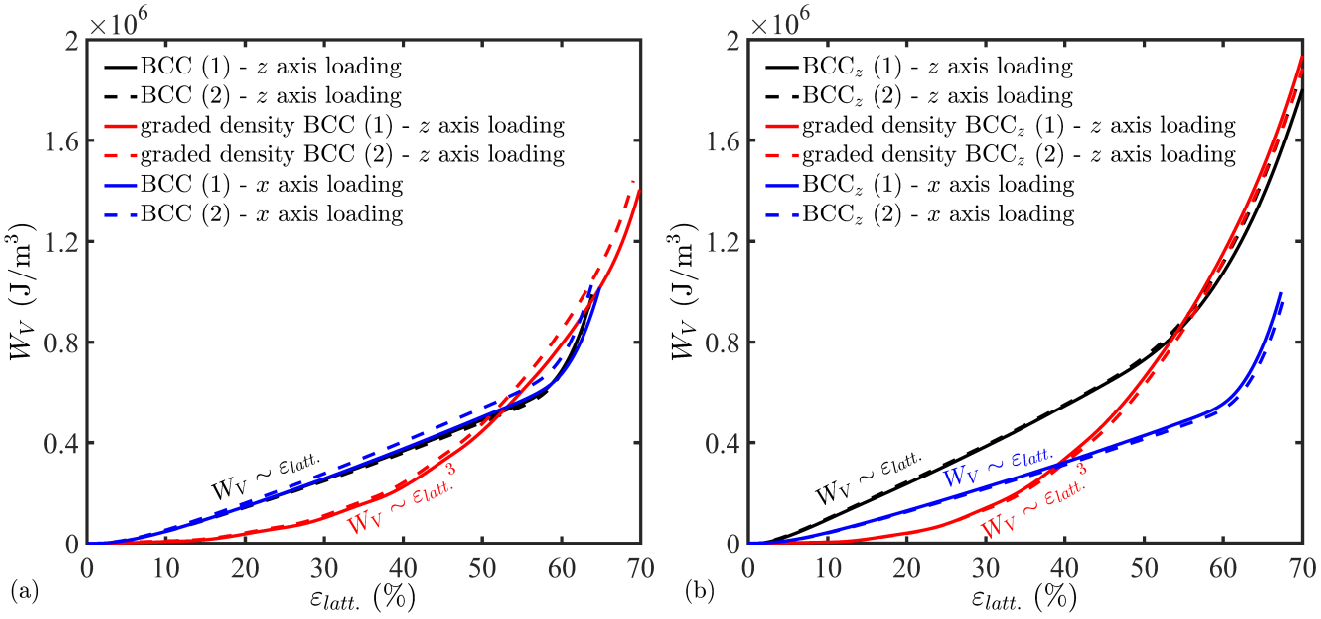

Figure 6. Cumulative energy absorption per unit volume for the BCC (a) and BCC$_z$ (b) lattice structures under compressive loading. The notation (1) and (2) in the legend refers to two samples of the same type, i.e. repeat tests.

than the non-graded structures, 1371 ± 9 kJ/m^3 vs. 640 ± 10 kJ/m^3. This represents a $(114 \pm 4)\%$ improvement in energy absorption, larger than the 80% seen for the BCC lattices. As for the BCC graded structures, the graded BCC$_z$ structures exhibited W_V behaviour that was roughly proportional to $\varepsilon_{latt.}{}^3$.

Figure 7 provides an alternative representation of energy absorption in the examined lattice structures. The cumulative energy per unit volume is normalised with the elastic modulus of the lattice strut material, $E_{sol.}$, and this is plotted against the stress, also normalised with $E_{sol.}$. This representation was used by Gibson and Ashby[1] to demonstrate the effect of relative density on the energy absorption processes of various foams. It is useful in allowing a designer to select a foam or lattice that minimises the stress while the required energy is absorbed.

Three regions, A, B and C, are denoted in figure 7. Region A corresponds to the initial elastic region of the non-graded structures, and also includes the collapse of the first two low-density layers of the graded structures. In this region only a small amount of the total energy is absorbed. In region B the non-graded structures enter their plastic plateaux,

Table 5. Densification strains, ε_D, and energy absorbed per unit volume at densification, W_{V_D}, for the BCC and BCC$_z$ lattice structures.

	BCC			BCC$_z$		
	z axis loading	x axis loading	graded density	z axis loading	x axis loading	graded density
ε_D (%)	53.46 ± 0.04	53.5 ± 0.4	63 ± 2	45.5 ± 0.8	55.8 ± 0.3	63.7 ± 0.4
W_{V_D} (kJ/m^3)	529 ± 6	570 ± 10	940 ± 50	640 ± 10	484 ± 5	1371 ± 9

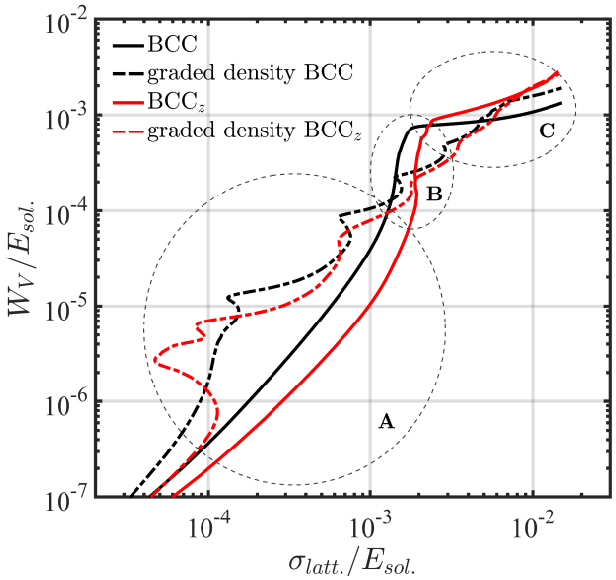

Figure 7. Normalised energy absorption of BCC and BCC$_z$ graded and non-graded lattices.

and so exhibit a drastic increase in absorbed energy with very little increase in stress. In the same region, the graded structures absorb energy at a lower rate, whilst continuing to experience periodic weakening due to the collapse of their cellular layers. Finally, in region C the non-graded structures enter the densification regime; this is evident in the turning point and subsequent rapid increase in stress. In comparison, the graded structures do not exhibit sharp turning points, but rather enter the densification regime more gradually, continuing to absorb energy at roughly the same rate as throughout their deformation.

Conclusions

An investigation was conducted into the deformation processes and mechanical performance of several functionally graded and non-graded lattice structures. The examined lattice types were the BCC and BCC$_z$, the latter of which had additional reinforcing struts in one direction. Comparing their mechanical properties revealed that BCC$_z$ lattices possess significant mechanical anisotropy, being weaker when loaded perpendicularly to their reinforcing struts, while BCC lattices are more isotropic. On the other hand, BCC$_z$ lattices loaded in their reinforced direction have superior modulus and plateau strength compared to BCC. Both non-graded lattice types exhibited stress-strain behaviour conventionally associated with repeating cellular solids such as foams, featuring long plateaux followed by densification. The energy absorbed by non-graded structures prior to densification increased linearly with compressive strain.

In contrast to the uniformly dense structures, functionally graded lattices showed distinctive stress-strain behaviour in which the structures were periodically weakened as their cellular layers collapsed in sequence, from the low density layers at the tops of the structures to the high density layers at their bases. This observation is in agreement with a previous report[24] and highlights how the lattice material distribution, even for structures of equivalent average density, can significantly affect the deformation behaviour. In another deviation from the performance of uniform density structures, the graded structures absorbed energy proportionally to $\varepsilon_{latt.}{}^3$. Their total energy absorption prior to the densification of their last layers was significantly higher than that of the non-graded structures.

The presentation in this paper of several Gibson-Ashby prefactors (C_1, C_5 and α of equation 1) for two types of lattice structure is a major contribution to the field of cellular solids research. These values facilitate the informed design of lattice structures for load bearing and energy absorption applications, and allow the development of constitutive models for an advanced MTO approach to lattice structure design. This research also demonstrates the potential for optimised functionally graded lattices to be manufactured by AM. The results indicate how functionally graded AM lattices can be used to engineer a progressive response to an applied dynamic or static load by controlling the stiffness and energy absorption as a function of deformation. These structures may therefore be of great benefit in applications demanding the controlled absorption of impact energy, for example in personal protection equipment where the maximum deceleration of a body must be minimised to prevent harm.

Acknowledgements

Thanks to Mark East, Mark Hardy, Joe White, Jason Greaves and Tom Buss.

Funding

The funding for this research was provided by the EPSRC.

References

1. Gibson L and Ashby M, *Cellular Solids: Structure and properties*. Cambridge University Press, 1997.
2. Ashby M et al., *Metal Foams: A Design Guide*. Butterworth-Heinemann, 2000.
3. Fleck NA, Deshpande VS and Ashby MF, Micro-architectured materials: past, present and future. *P Roy Soc Lond A - Mat* 2010; 466:2495 – 2516.
4. Lu T, Stone H and Ashby M, Heat transfer in open-cell metal foams. *Acta Mater* 1998; 46:3619 – 3635.
5. Mines R et al., Drop weight impact behaviour of sandwich panels with metallic micro lattice cores. *Int J Impact Eng* 2013; 60:120 – 132.
6. Fuller AJ et al., Measurement and interpretation of the heat transfer coefficients of metal foams. *P I Mech Eng C -J Mec* 2005; 219:183 – 191.
7. Wadley H et al., Compressive response of multilayered pyramidal lattices during underwater shock loading. *Int J Impact Eng* 2008; 35:1102 – 1114.
8. Wadley H, Multifunctional periodic cellular metals. *Phil Trans R Soc A* 2006; 364:31 – 68.
9. Wang B and Cheng G, Design of cellular structures for optimum efficiency of heat dissipation. *Struct Multidiscip O* 2005; 30:447 – 458.
10. Seepersad C et al., Multifunctional Topology Design of Cellular Material Structures. *ASME J Mech Des* 2008; 130:31404.
11. Evans A et al., The topological design of multifunctional cellular metals. *Prog Mater Sci* 2001; 46:309 – 327.
12. Wen T et al., Forced convection in metallic honeycomb structures. *Int J Heat Mass Tran* 2006; 49:3313 – 3324.
13. Wadley H and Queheillalt D, Thermal Applications of Cellular Lattice Structures. *Mat Sci Forum* 2007; 539 - 543:242 247.
14. Gama BA et al., Aluminum foam integral armor: a new dimension in armor design. *Compos Struct* 2001; 52:381 – 395, design and Manufacturing of Composite Structures.
15. Brennan-Craddock J et al., The design of impact absorbing structures for additive manufacture. *J Phys: Conference Series* 2012; 382:012042.
16. Hangai Y et al., Fabrication of functionally graded aluminum foam using aluminum alloy die castings by friction stir processing. *Mat Sci Eng A - Struct* 2012; 534:716 – 719.
17. Brothers AH and Dunand DC, Mechanical properties of a density-graded replicated aluminum foam. *Mat Sci Eng A - Struct* 2008; 489:439 – 443.
18. Hassani A, Habibolahzadeh A and Bafti H, Production of graded aluminum foams via powder space holder technique. *Mater Design* 2012; 40:510 – 515.
19. Heim HP and Tromm M, Injection molded components with functionally graded foam structures Procedure and essential results. *J Cell Plast* 2015; 0:1 – 21.
20. Tissandier C, González-Núñez R and Rodrigue D, Asymmetric microcellular composites: Morphological properties. *J Cell Plast* 2014; 50:449 – 473.
21. Zhang Xc, An Lq and Ding Hm, Dynamic crushing behavior and energy absorption of honeycombs with density gradient. *J Sandw Struct Mater* 2014; 16:125–147.
22. Mousanezhad D et al., Impact resistance and energy absorption of regular and functionally graded hexagonal honeycombs with cell wall material strain hardening. *Int J Mech Sci* 2014; 89:413 – 422.
23. Mosanenzadeh SG et al., Design and development of novel bio-based functionally graded foams for enhanced acoustic capabilities. *J Mater Sci* 2015; 50:1248–1256.
24. van Grunsven W et al., Fabrication and Mechanical Characterisation of Titanium Lattices with Graded Porosity. *Metals* 2014; 4:401 – 409.
25. Miltz J and Ramon O, Energy Absorption Characteristics of Polymeric Foams Used as Cushioning Materials. *Polym Eng Sci* 1990; 30:129 – 133.
26. Li QM, Magkiriadis I and Harrigan JJ, Compressive Strain at the Onset of Densification of Cellular Solids. *J Cell Plast* 2006; 42:371 – 392.
27. Ngim D, Liu JS and Soar R, Design optimization of consolidated granular-solid polymer prismatic beam using metamorphic development. *Int J Solids Struct* 2009; 46:726 – 740.